Correspondence between a plasma-based EMIC wave proxy and subauroral proton precipitation

M. Spasojevic,[1,2] L. W. Blum,[3] E. A. MacDonald,[4] S. A. Fuselier,[2] and D. I. Golden[1]

Received 20 September 2011; revised 4 November 2011; accepted 4 November 2011; published 13 December 2011.

[1] The loss of relativistic electrons from the Earth's radiation belts as a result of resonant interactions with electromagnetic ion cyclotron waves (EMIC) waves has yet to be fully quantified, in part, due to the lack of global measurements of the wave distribution during individual storm events. Recent work has focused on augmenting direct wave measurements with proxy wave indicators. Here we compare two different techniques for inferring the presence of EMIC waves: 1) a wave-growth proxy and amplitude estimate based on in situ plasma measurements of the cold and hot ion distributions, and 2) FUV observations of subauroral proton precipitation, which is thought to result from interactions with EMIC waves. For two event intervals, we show good correspondence between proxy predictions of wave growth, calculated using measurements from geostationary spacecraft, and precipitation observed at the northern hemisphere ionospheric footprint. Further, for times when the proxy is positive, we observe a moderate positive correlation (r = 0.56) between the predicted wave amplitude and the mean FUV brightness in a 300-km circle about the footprint. Further development and verification of these techniques will enhance our ability to infer the global distribution of EMIC waves when direct measurements are not available.
Citation: Spasojevic, M., L. W. Blum, E. A. MacDonald, S. A. Fuselier, and D. I. Golden (2011), Correspondence between a plasma-based EMIC wave proxy and subauroral proton precipitation, *Geophys. Res. Lett.*, *38*, L23102, doi:10.1029/2011GL049735.

1. Introduction

[2] Wave-induced pitch angle scattering is believed to be one of primary physical processes that drives the loss of relativistic electrons within the Earth's radiations belts [e.g., *Millan and Thorne*, 2007]. However, the overall contribution of pitch angle scattering to electron lifetimes and the relative contribution of the multitude of individual wave modes has yet to be quantified. A major challenge is that the evolution of electron fluxes is dependent on competition among a variety of acceleration and losses processes resulting in wide variability in the dynamics during individual geomagnetic storms [e.g., *Reeves et al.*, 2003]. Progress in this area has been further hampered by a dearth of in situ plasma wave measurements from solar cycle 23.

[3] Electromagnetic ion cyclotron (EMIC) waves can, through anomalous resonance, interact with highly energetic electrons (>1 MeV), and it has been suggested that these waves are responsible for the rapid depletion of relativistic electron flux during the main phase of some geomagnetic storms [*Bortnik et al.*, 2006; *Millan et al.*, 2007]. Some statistical distributions of EMIC waves are available from earlier spacecraft missions [*Anderson et al.*, 1992; *Fraser and Nguyen*, 2001; *Meredith et al.*, 2003], but progress in quantifying wave scattering requires knowledge of how the wave distribution evolves spatially over the course of a storm.

[4] EMIC wave growth is driven by anisotropic ($T_\perp > T_\parallel$) ring current ion distributions. If the anisotropy is sufficiently large, waves grow and scatter protons so as to reduce the anisotropy and stabilize the distribution. In addition, the critical anisotropy required for wave growth is reduced in the regions of enhanced cold plasma such as in the plasmasphere and plume regions [*Cornwall et al.*, 1970]. Wave growth results in the precipitation of protons into the upper atmosphere, and there is a considerable body of experimental work relating EMIC waves to proton precipitation such as measured by particle detectors or auroral imagers, particularly in the dusk sector plasmasphere/ring current overlap region [e.g., *Erlandson and Ukhorskiy*, 2001; *Fraser et al.*, 2006; *Yahnin and Yahnina*, 2007; *Sakaguchi et al.*, 2008]. *Spasojevic and Fuselier* [2009] examined global images of the proton aurora and plasmasphere and suggested that the location and duration of precipitation associated with the plasmasphere could be used as an indirect measure of the occurrence of EMIC waves.

[5] *Blum et al.* [2009] developed a proxy to infer the occurrence of enhanced EMIC waves using in situ plasma measurements from geosynchronous orbit. In a superposed epoch analysis of storm intervals, they found that for storms resulting in net relativistic electron loss, the EMIC wave proxy predicts a greater occurrence of enhanced EMIC waves especially during the recovery phase of storms, implying that the EMIC waves may be a driver of this loss. However, since the spacecraft used to compute the proxy do not make simultaneous measurements of waves, it has not been possible to directly verify the efficacy of the proxy in predicting the presence of EMIC waves.

[6] In this paper, we extend the *Blum et al.* [2009] proxy to estimate wave amplitude based on expectations from linear theory and compare the predictions of the proxy with the spatial and temporal evolution of subauroral proton precipitation observed by a global aurora imager for two event intervals. We show that the onset of wave growth as estimated from the proxy using plasma measurements from the geostationary spacecraft 1994–084 and LANL-97A is well correlated with proton precipitation at the northern magnetic field line footprint of that same spacecraft, as measured by

[1]Space, Telecommunications and Radioscience Laboratory, Stanford University, Stanford, California, USA.
[2]Lockheed Martin Advanced Technology Center, Palo Alto, California, USA.
[3]Laboratory for Atmospheric and Space Physics, University of Colorado at Boulder, Boulder, Colorado, USA.
[4]Los Alamos National Laboratory, Los Alamos, New Mexico, USA.

0094-8276/11/2011GL049735

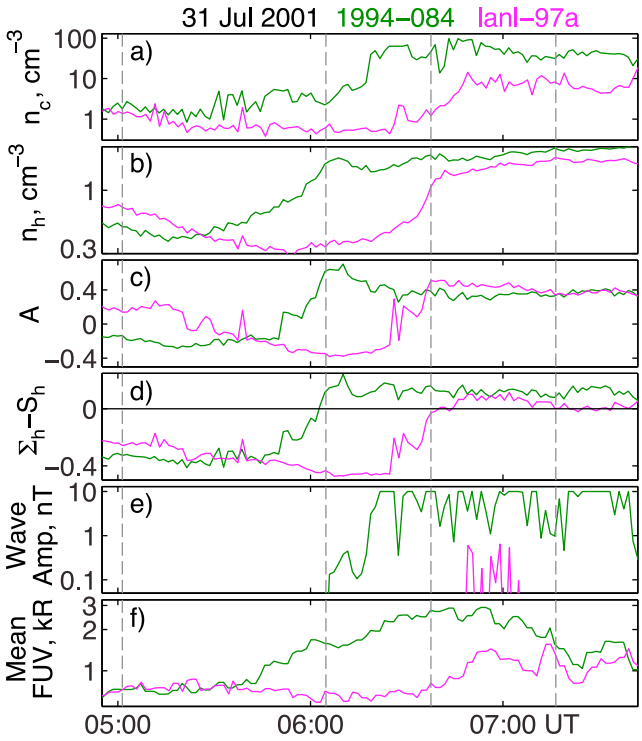

Figure 1. For geostationary spacecraft 1994–084 (magenta) and LANL-97a (green): (a) cold (1–100 eV/q) ion density (log scale), (b) hot (0.1–45 keV/q) ion density (log scale), (c) hot ion temperature anisotropy ($A = T_\perp/T_\parallel - 1$), (d) EMIC wave proxy, $\Sigma_h - S_h$, (e) estimated EMIC wave amplitude (log scale), and (f) mean FUV brightness in a 300-km circle around the magnetic footprint of the spacecraft as detected by the IMAGE FUV SI12 instrument (log scale). The vertical dashed lines correspond to the times of the FUV images in Figure 2, and the dashed line at 06:37 UT also corresponds to storm minimum *SYM-H*.

the IMAGE FUV instrument. In the first event, the geostationary spacecraft appear to move into a pre-existing region of wave activity whereas in the second event, a temporal enhancement in wave activity is observed. We also find quantitative agreement between the wave amplitude and the intensity of precipitation with the interval of most intense precipitation corresponding to the highest predicted wave amplitudes. Further application of these techniques will enhance our ability to accurately infer the global distribution of EMIC waves from indirect measures.

2. EMIC Wave Proxy and Amplitude Estimation

[7] Linear theory predicts that the EMIC instability imposes an upper bound on the proton temperature anisotropy, which scales as a function of plasma β in the form

$$\frac{T_{\perp h}}{T_{\parallel h}} - 1 = \frac{S_h}{\beta_{\parallel h}^{\alpha_h}} \tag{1}$$

where $\beta_{\parallel h} = 8\pi n_h T_{\parallel h}/B_\circ^2$. For a given value of the local growth rate (γ/Ω_p), the parameters S_h and α_h can be expressed solely as functions of the relative fraction of hot protons, $n_h/(n_c + n_h)$ [*Gary et al.*, 1994].

[8] The *Blum et al.* [2009] wave proxy compares the theoretical instability threshold, S_h, to an observational parameter based on in situ plasma measurements, Σ_h.

$$\Sigma_h = \left(\frac{T_{\perp h}}{T_{\parallel h}} - 1\right)\beta_{\parallel h}^{\alpha_h} \tag{2}$$

Σ_h is determined using the values of n_c, n_h, T_h, and $T_{\parallel h}$ calculated from the moments of the ion distributions measured by the Magnetospheric Plasma Analyzer (MPA) instrument [*Bame et al.*, 1993] onboard geostationary spacecraft along with an estimate of B° [*Tsyganenko and Sitnov*, 2005] and the fitting function for α_h [*Blum et al.*, 2009]. For a given measurement interval, S_h is calculated for a minimum expected value of $\gamma/\Omega_p = 0.001$. If $\Sigma_h - S_h < 0$, the distribution of hot protons is expected to be stable against the cyclotron instability while wave growth is expected for $\Sigma_h - S_h > 0$.

[9] We extend the wave proxy to estimate EMIC wave amplitude, a key parameter for evaluating wave-particle interactions. For intervals when $\Sigma_h - S_h > 0$ for $\gamma/\Omega_p = 0.001$, we scale the value of γ/Ω_p in the range 0.001 to 0.01, essentially finding the growth rate for which $S_h \approx \Sigma_h$. Next, using the warm plasma dispersion relation [*Kozyra et al.*, 1984], the wave group velocity and thus convective growth rate (γ/v_g) is calculated. The convective growth rate is integrated along the source region to obtain a total wave gain, G [*Jordanova et al.*, 2001]. We assume parallel propagation in a dipole field and that the growth rate and group velocity are constant along the source region, which extends $\pm 10°$ of the equator. Finally, we scale the gain to calculate a wave amplitude using $B_w = 10 \times 10^{(G-40)/13}$ nT. For $G < 13$ dB ($B_w < 0.08$ nT), we consider wave growth negligible, and for $G > 40$ dB ($B_w = 10$ nT), we assume saturation.

3. Observations

[10] We examine two intervals for which the wave proxy predicts EMIC growth: 1) 31 Jul 2001, a minor geomagnetic storm and 2) 24 Jul 2001, a recovery period substorm. During this time the FUV SI12 global proton auroral imager [*Mende et al.*, 2000] was operating onboard the IMAGE spacecraft [*Burch*, 2000]. During the two intervals examined here, SI12 observed the formation of afternoon detached subauroral arcs, which are primarily a storm-time phenomenon associated with EMIC wave scattering of ring current protons along the plasmapause boundary or within plasmaspheric plumes [*Jordanova et al.*, 2007; *Spasojevic and Fuselier*, 2009].

[11] During the peak of the 31 Jul 2001 storm (SYM-H_{min} = −51 nT at 06:37 UT), geostationary spacecraft 1994–084 and LANL-97a were on the dayside. As they traveled to later magnetic local time, the spacecraft successively encountered a region of enhanced cold and hot ion density and hot ion temperature anisotropy (Figures 1a–1c). The EMIC wave proxy predicts enhanced waves ($\Sigma_h - S_h > 0$) starting near 6 UT (13 MLT) for 1994–084 and near 6:40 UT (11.4 MLT) for LANL-97A (Figure 1d) corresponding to the increase in n_h and A. However, appreciable wave amplitudes are not predicted until each spacecraft enters the plasmaspheric plume resulting in lower wave v_g and thus higher convective growth rates.

[12] Figure 2 shows a sequence of IMAGE FUV SI12 images of the proton aurora in the northern hemisphere ionosphere that capture the formation of an afternoon detached

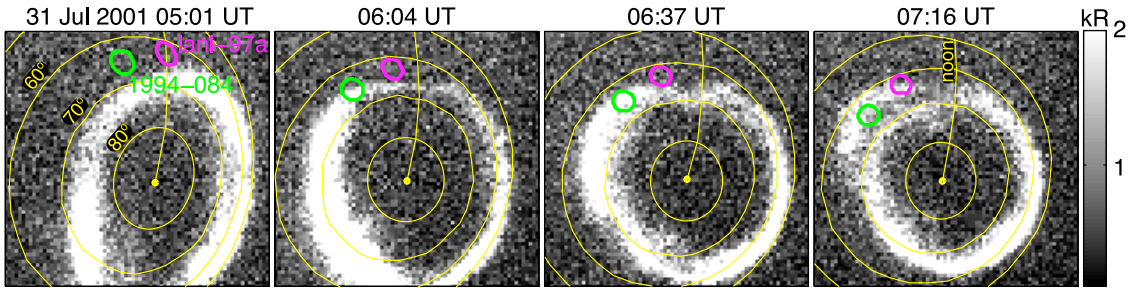

Figure 2. Sequence of IMAGE FUV SI12 images of the proton aurora along with 300-km circles drawn around the magnetic field line footprint of the geostationary spacecraft 1994–084 and lanl–97a. The latitude circles are geomagnetic and the 12 MLT meridian is indicated. These times correspond to the dashed vertical lines in Figure 1.

subauroral arc. In the aftermath of a northward IMF turning, the broad region of intense proton precipitation in the post-noon quadrant evolves into two distinct arcs with the main proton oval at high latitudes and latitudinally separated subauroral arc, which maps to the plasmapause and plume region as determined from global EUV images [*Spasojevic and Fuselier*, 2009].

[13] Also shown in Figure 2 are circles 300-km in radius about the magnetic field line footprints of the two geostationary spacecraft calculated using the *Tsyganenko and Sitnov* [2005] field model and the *Qin et al.* [2007] solar wind parameters. Over time, the footprints of the two spacecraft move into the region of enhanced duskside proton precipitation that evolves into the detached arc. Figure 1f shows the mean FUV brightness within a 300-km circle of the estimated footprint from the nearest-in-time FUV image. Footprints were also calculated with a set of field models [*Tsyganenko*, 1989; *Tsyganenko and Stern*, 1996; *Ostapenko and Maltsev*, 1997; *Tsyganenko*, 2002] and found to be within 120 km of the value used here. Examining the FUV intensity within a 300-km circle of the footprint takes into account uncertainty associated with the magnetic field mapping as well as additional uncertainty associated with the FUV camera pointing. Within the footprints of the two spacecraft, FUV observes an increase in proton precipitation within ± 10 minutes of when $\Sigma_h - S_h$ becomes positive. In addition, there is a general correlation between the intensity of the FUV precipitation and predicted amplitude of the waves with the intense waves predicted by 1994–084 corresponding to the more intense precipitation and the weaker waves predicted by LANL-97a corresponding to weaker precipitation.

[14] In the second interval, on 24 Jul 2001 near 7 UT, the proxy predicts EMIC waves as a result of an isolated substorm injection during a period of enhanced solar wind dynamic pressure ($P_{sw} \approx 5.5$ nPa). Beginning after 8 UT, 1994–084 (located near 15 MLT) observed an approximately simultaneous increase in n_c, n_h, and A (not shown) leading to $\Sigma_h - S_h > 0$ for about 70 mins (Figure 3c). The predicted wave amplitudes are shown in Figure 3d. As in the previous case, when the proxy is positive, higher wave amplitudes are predicted in the regions of higher cold plasma density. Unfortunately, for this event, no data are available from the nearby LANL-97A spacecraft.

[15] During this time, IMAGE FUV observes the formation of a detached subauroral arc (Figure 3). Prior to the period of enhanced wave growth predicted by the proxy, the footprint of 1994–084 maps to a dim region devoid of proton precipitation (Figure 3a), but later when wave growth is predicted, the spacecraft maps directly to the region of precipitation that has formed at subauroral latitudes (Figure 3b). The predicted wave amplitudes are on the same order (~0.1–1 nT) as those predicted for LANL-97a in the previous case (Figure 2e, green curve), and similarly when the proxy is positive the mean FUV brightness is also on the same order (~1–1.5 kR).

4. Discussion

[16] Examining global patterns of subauroral proton precipitation in conjunction with the plasma-based EMIC wave proxy allows us to separate spatial and temporal changes in the global wave pattern. For example, in the 31 Jul 2001 storm event, the duskside proton oval had expanded and moved to lower latitude by 05:30 UT. Thus, the leading spacecraft, 1994–084, moves into a pre-existing precipitation region (Figure 2b). The precipitation region subsequently begins to expand to lower latitude and earlier local time such that the trailing spacecraft, LANL-97a, enters the precipitation

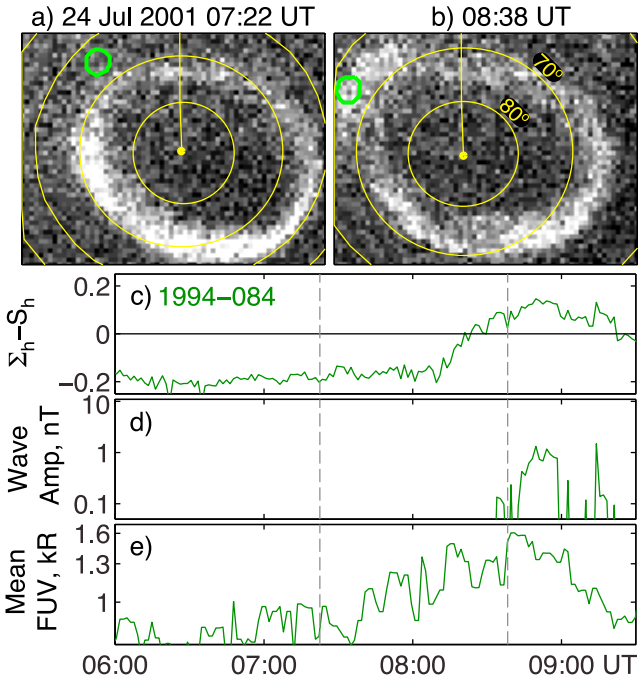

Figure 3. For 24 Jul 2001: (a and b) Same as Figure 2 with the identical colorscale. (c–e) Same as Figures 1d–1f.

region about 40 mins after the leading spacecraft despite being >2 hours behind in local time. In contrast, for the 24 Jul 2001 substorm event, the subauroral arc essentially forms under the footprint of the spacecraft in response to a fresh injection of energetic substorm protons, and the temporal duration of the elevated wave proxy is consistent with the temporal duration of the subauroral proton precipitation.

[17] For the two events presented here, we have found good correspondence between proxy predictions of EMIC growth and proton precipitation within the field line footprint. For times when the proxy is positive, we observe a moderate positive correlation (r = 0.56) between the predicted wave amplitude and the mean FUV brightness in the footprint area. A relationship between precipitation and wave intensity (rather than just wave growth) is expected since in treating the wave-particle interaction as a quasi-linear process, the pitch angle diffusion rate is function of wave amplitude [*Kennel and Petschek*, 1966]. The agreement between wave amplitude and FUV brightness is, of course, not perfect demonstrating the uncertainty associated with using either of these measures to infer the wave distribution. For example, towards the end of the study interval on 31 Jul 2001, 1994–084 continues to predict wave amplitudes near 10 nT as a result of continued observation of enhanced cold ion density, hot ion density and hot ion temperature anisotropy, but the precipitation at the footprint is gradually decreasing (Figures 2e and 2f). However, given the considerable number of assumptions upon which the proxy and wave amplitude predictions are based and the challenges in comparing those quantities to data from the ionospheric footprint, the correspondence between the proxy predictions and the FUV brightness is rather remarkable. These results demonstrate the efficacy of proxy measures, and future work will focus on statistical comparison of the Los Alamos and IMAGE/FUV databases along with improved quantification of the proxy conversion to estimated wave power.

[18] To ultimately quantify the relative role of wave-particle interactions in the evolution of radiation belt electron fluxes, the global spatial distribution of all relevant wave modes as a function of time for individual storm events is required. Currently, the spatial distribution of EMIC waves is very poorly understood, and information regarding wave occurrence as a function of storm phase is contradictory. In analyzing ground-based observations of EMIC waves in conjunction with low altitude satellite observations of precipitating protons in the 30–80 keV range, *Engebretson et al.* [2008] concluded that EMIC waves primarily occur during the storm recovery phase and are absent in early phases. In contrast, two studies of in situ EMIC observations by *Fraser et al.* [2010] (using GOES data) and *Halford et al.* [2010] (using CRRES data) found a predominance of wave activity during main phase. The case event of the storm on July 31, 2001 presented here is more inline with the latter studies, as the waves are predicted within about 45 mins of minimum storm *SYM-H*.

[19] Multi-point wave measurements, such as those proposed by the dual-spacecraft Radiation Belt Storm Probes mission, will provide some missing pieces of the global wave map, and wave proxies hold promise for filling in the gaps. Wave proxies based on in situ plasma measurements, including the EMIC proxy discussed here and the whistler mode proxy developed by *MacDonald et al.* [2008], have the advantage of utilizing existing space-based assets with simultaneous measurements distributed in local time and long term observational databases.

[20] **Acknowledgments.** The work at Lockheed Martin was support by NASA award NNX07AG52G. The work at University of Colorado, Boulder was supported by NSF ATM-0842388. The work at Los Alamos was supported by the Radiation Belt Storm Probes Energetic particle, Composition, and Thermal plasma science investigation under NASA contract award 923497 and was performed under the auspices of the U.S. Department of Energy (DOE).

[21] The Editor thanks two anonymous reviewers for their assistance in evaluating this paper.

References

Anderson, B. J., R. E. Erlandson, and L. J. Zanetti (1992), A statistical study of Pc 1–2 magnetic pulsations in the equatorial magnetosphere: 1. Equatorial occurrence distributions, *J. Geophys. Res.*, *97*(A3), 3075, doi:10.1029/91JA02706.

Bame, S. J., et al. (1993), Magnetospheric plasma analyzer for spacecraft with constrained resources, *Rev. Sci. Instrum.*, *64*, 1026, doi:10.1063/1.1144173.

Blum, L. W., E. A. MacDonald, S. P. Gary, M. F. Thomsen, and H. E. Spence (2009), Ion observations from geosynchronous orbit as a proxy for ion cyclotron wave growth during storm times, *J. Geophys. Res.*, *114*, A10214, doi:10.1029/2009JA014396.

Bortnik, J., R. M. Thorne, T. P. O'Brien, J. C. Green, R. J. Strangeway, Y. Y. Shprits, and D. N. Baker (2006), Observation of two distinct, rapid loss mechanisms during the 20 November 2003 radiation belt dropout event, *J. Geophys. Res.*, *111*, A12216, doi:10.1029/2006JA011802.

Burch, J. L. (2000), Image mission overview, *Space Sci. Rev.*, *91*, 1.

Cornwall, J. M., F. V. Coroniti, and R. M. Thorne (1970), Turbulent loss of ring current protons, *J. Geophys. Res.*, *75*, 4699, doi:10.1029/JA075i025p04699.

Engebretson, M. J., et al. (2008), Pc1–Pc2 waves and energetic particle precipitation during and after magnetic storms: Superposed epoch analysis and case studies, *J. Geophys. Res.*, *113*, A01211, doi:10.1029/2007JA012362.

Erlandson, R. E., and A. J. Ukhorskiy (2001), Observations of electromagnetic ion cyclotron waves during geomagnetic storms: Wave occurrence and pitch angle scattering, *J. Geophys. Res.*, *106*, 3883, doi:10.1029/2000JA000083.

Fraser, B. J., and T. S. Nguyen (2001), Is the plasmapause a preferred source region of electromagnetic ion cyclotron waves in the magnetosphere?, *J. Atmos. Sol. Terr. Phys.*, *63*, 1225, doi:10.1016/S1364-6826(00)00225-X.

Fraser, B. J., T. M. Loto'Aniu, and H. J. Singer (2006), Electromagnetic ion cyclotron waves in the magnetosphere, in *Magnetospheric ULF Waves: Synthesis and New Directions*, *Geophys. Monogr. Ser.*, vol. 169, edited by K. Takahashi et al., p. 195, AGU, Washington, D. C.

Fraser, B. J., R. S. Grew, S. K. Morley, J. C. Green, H. J. Singer, T. M. Loto'aniu, and M. F. Thomsen (2010), Storm time observations of electromagnetic ion cyclotron waves at geosynchronous orbit: GOES results, *J. Geophys. Res.*, *115*, A05208, doi:10.1029/2009JA014516.

Gary, S. P., M. B. Moldwin, M. F. Thomsen, D. Winske, and D. J. McComas (1994), Hot proton anisotropies and cool proton temperatures in the outer magnetosphere, *J. Geophys. Res.*, *99*, 23,603, doi:10.1029/94JA02069.

Halford, A. J., B. J. Fraser, and S. K. Morley (2010), EMIC wave activity during geomagnetic storm and nonstorm periods: CRRES results, *J. Geophys. Res.*, *115*, A12248, doi:10.1029/2010JA015716.

Jordanova, V. K., C. J. Farrugia, R. M. Thorne, G. V. Khazanov, G. Reeves, and M. F. Thomsen (2001), Modeling ring current proton precipitation by electromagnetic ion cyclotron waves during the May 14–16, 1997, storm, *J. Geophys. Res.*, *106*, 7, doi:10.1029/2000JA002008.

Jordanova, V. K., M. Spasojevic, and M. F. Thomsen (2007), Modeling the electromagnetic ion cyclotron wave-induced formation of detached subauroral proton arcs, *J. Geophys. Res.*, *112*, A08209, doi:10.1029/2006JA012215.

Kennel, C. F., and H. E. Petschek (1966), Limit on stably trapped particle fluxes, *J. Geophys. Res.*, *71*, 1.

Kozyra, J. U., T. E. Cravens, A. F. Nagy, E. G. Fontheim, and R. S. B. Ong (1984), Effects of energetic heavy ions on electromagnetic ion cyclotron wave generation in the plasmapause region, *J. Geophys. Res.*, *89*, 2217, doi:10.1029/JA089iA04p02217.

MacDonald, E. A., M. H. Denton, M. F. Thomsen, and S. P. Gary (2008), Superposed epoch analysis of a whistler instability criterion at geosynchronous orbit during geomagnetic storms, *J. Atmos. Sol. Terr. Phys.*, *70*, 1789, doi:10.1016/j.jastp.2008.03.021.

Mende, S. B., et al. (2000), Far ultraviolet imaging from the image spacecraft. 3. spectral imaging of lyman-α and oi 135.6 nm, *Space Sci. Rev.*, *91*, 287.

Meredith, N. P., R. M. Thorne, R. B. Horne, D. Summers, B. J. Fraser, and R. R. Anderson (2003), Statistical analysis of relativistic electron energies for cyclotron resonance with EMIC waves observed on CRRES, *J. Geophys. Res.*, *108*(A6), 1250, doi:10.1029/2002JA009700.

Millan, R. M., and R. M. Thorne (2007), Review of radiation belt relativistic electron losses, *J. Atmos. Sol. Terr. Phys.*, *69*, 362, doi:10.1016/j.jastp.2006.06.019.

Millan, R. M., R. P. Lin, D. M. Smith, and M. P. McCarthy (2007), Observation of relativistic electron precipitation during a rapid decrease of trapped relativistic electron flux, *Geophys. Res. Lett.*, *34*, L10101, doi:10.1029/2006GL028653.

Ostapenko, A. A., and Y. P. Maltsev (1997), Relation of the magnetic field in the magnetosphere to the geomagnetic and solar wind activity, *J. Geophys. Res.*, *102*, 17,467, doi:10.1029/97JA00937.

Qin, Z., R. E. Denton, N. A. Tsyganenko, and S. Wolf (2007), Solar wind parameters for magnetospheric magnetic field modeling, *Space Weather*, *5*, S11003, doi:10.1029/2006SW000296.

Reeves, G. D., K. L. McAdams, R. H. W. Friedel, and T. P. O'Brien (2003), Acceleration and loss of relativistic electrons during geomagnetic storms, *Geophys. Res. Lett.*, *30*(10), 1529, doi:10.1029/2002GL016513.

Sakaguchi, K., K. Shiokawa, Y. Miyoshi, Y. Otsuka, T. Ogawa, K. Asamura, and M. Connors (2008), Simultaneous appearance of isolated auroral arcs and Pc 1 geomagnetic pulsations at subauroral latitudes, *J. Geophys. Res.*, *113*, A05201, doi:10.1029/2007JA012888.

Spasojevic, M., and S. A. Fuselier (2009), Temporal evolution of proton precipitation associated with the plasmaspheric plume, *J. Geophys. Res.*, *114*, A12201, doi:10.1029/2009JA014530.

Tsyganenko, N. A. (1989), A magnetospheric magnetic field model with a warped tail current sheet, *Planet. Space Sci.*, *37*, 5, doi:10.1016/0032-0633(89)90066-4.

Tsyganenko, N. A. (2002), A model of the near magnetosphere with a dawn-dusk asymmetry: 1. Mathematical structure, *J. Geophys. Res.*, *107*(A8), 1179, doi:10.1029/2001JA000219.

Tsyganenko, N. A., and M. I. Sitnov (2005), Modeling the dynamics of the inner magnetosphere during strong geomagnetic storms, *J. Geophys. Res.*, *110*, A03208, doi:10.1029/2004JA010798.

Tsyganenko, N. A., and D. P. Stern (1996), Modeling the global magnetic field of the large-scale birkeland current systems, *J. Geophys. Res.*, *101*, 27,187, doi:10.1029/96JA02735.

Yahnin, A., and T. A. Yahnina (2007), Energetic proton precipitation related to ion cyclotron waves, *J. Atmos. Sol. Terr. Phys.*, *69*, 1690, doi:10.1016/j.jastp.2007.02.010.

L. W. Blum, Laboratory for Atmospheric and Space Physics, University of Colorado at Boulder, Boulder, CO 80303, USA.

S. A. Fuselier, Lockheed Martin Advanced Technology Center, Palo Alto, CA 94304, USA.

D. I. Golden and M. Spasojevic, Space, Telecommunications and Radioscience Laboratory, Stanford University, Stanford, CA 94305, USA. (mariaspasojevic@stanford.edu)

E. A. MacDonald, Los Alamos National Laboratory, Los Alamos, NM 87544, USA.